Journal of Molecular Spectroscopy **208,** 43–50 (2001)
doi:10.1006/jmsp.2001.8374, available online at http://www.idealibrary.com on IDEAL®

The Water Vapor Spectrum in the Region 8600–15 000 cm^{-1}: Experimental and Theoretical Studies for a New Spectral Line Database

II. Linelist Construction

Roland Schermaul,* Richard C. M. Learner,*,[1] David A. Newnham,† John Ballard,† Nikolai F. Zobov,‡,[2] Djedjiga Belmiloud,† and Jonathan Tennyson‡

*Laser Optics and Spectroscopy, Blackett Laboratory, Imperial College of Science, Technology and Medicine, Prince Consort Road, London SW7 2BW, United Kingdom; †Atmospheric Science Division, Space Science and Technology Department, Rutherford Appleton Laboratory, Chilton, Didcot, Oxfordshire OX11 0QX, United Kingdom; and ‡Department of Physics and Astronomy, University College London, Gower Street, London WC1E 6BT, United Kingdom

E-mail: david.newnham@rl.ac.uk, j.ballard@rl.ac.uk, j.tennyson@ucl.ac.uk

Received November 30, 2000; in revised form April 26, 2001

The new laboratory measurements of R. Schermaul *et al.* (*J. Mol. Spectrosc.* **208**), for the near-infrared and visible spectrum of water vapor, covering the $2\nu + \delta$, 3ν, $3\nu + \delta$, and 4ν polyads, are combined with accurate calculations of weaker lines to provide a new, comprehensive linelist of water transitions for the spectral region 8600–15 000 cm^{-1}. The resulting ESA–WVR linelist reproduces the raw laboratory observations to a high level of agreement at all but the longest wavelengths. This linelist has been made available in a standard format for general use.

Key Words: water vapor; near-infrared and visible spectrum; line intensities; database.

1. INTRODUCTION

Reliable models of radiative transfer through water vapor are crucial for many applications, particularly models of the Earth's atmosphere. For this reason reliable spectroscopic data on water is considered vital for any database compilation. Standard databases such as HITRAN (*1*) and GEISA (*2*) rely heavily on long pathlength Fourier transform spectra recorded in the 1980s (*3–6*). A recent combined experimental and theoretical analysis of the near-infrared and visible spectrum of water showed that for the important $2\nu + \delta$, 3ν, $3\nu + \delta$, and 4ν polyads, covering the spectral region 8600–15 000 cm^{-1}, the line intensities obtained in earlier work and used in essentially all database compilations systematically underestimate the overall absorption of the polyads (*7*). This conclusion is unaltered by the recent corrections (*8*) to the water data used in HITRAN. Although Belmiloud *et al.* (*7*) gave overall scale factors for each polyad analyzed, they recognized that the proper solution required a remeasurement of the intensity of each line.

In the previous paper (*9*), henceforth known as I, we performed a systematic and thorough remeasurement of the air-broadened water spectrum in the range 8600–15 000 cm^{-1}, resulting in line parameters for some 4200 transitions. These lines make an excellent starting point for a new database on water transitions in this region; however, Learner *et al.* (*10*) showed that lines weaker than those readily measured in the laboratory can make a significant difference to the Earth's energy budget. A linelist of sufficient completeness cannot, therefore, be compiled from experimental data alone, and a dual approach, in which the strong line data are derived from experiment and the weak lines from theory is essential. For this reason we augment the list of stronger measured lines with theoretical estimates of the line parameters for the weaker lines. The result is a comprehensive database of over 36 000 water transitions which can be validated against the raw laboratory spectra. As will be shown, this validation process supports our strong line–weak line approach to the problem.

2. LINE PARAMETERS FROM THEORETICALLY DERIVED DATA

From a theoretical point of view the determination of line parameters for water divides into two parts: parameters which are an intrinsic property of the molecule, i.e., line positions and transition intensities, and those which depend on the molecular environment, i.e., line profiles and pressure shifts. While the theory for calculating the molecular properties has made great progress, the theory of pressure effects is much less secure. The present study therefore made use of computed line positions and

[1] Deceased.

[2] Permanent address: Institute of Applied Physics, Russian Academy of Science, Uljanov Street 46, Nizhnii Novgorod, Russia 603024.

0022-2852/01 $35.00

intensities for weak transitions, parameters for strong transitions being determined from the experimental measurements of I. Empirical procedures were used to characterize the line profiles of all transitions. This approximation is unlikely to limit practical applications as only the weak lines are treated in this fashion and line profiles are only of critical importance when a transition approaches saturation.

There are three considerations which determine the accuracy of the theoretical linelists used in the present study: the accuracy of the potential energy surface used (including any allowance made for the failure of the Born–Oppenheimer approximation), the accuracy of the dipole surface used, and the accuracy to which the nuclear motion calculations can be solved. In the present study, the error introduced by the nuclear motion procedures is insignificant and will not be considered further.

At present it is not possible to calculate a spectroscopically accurate Born–Oppenheimer potential energy surface for water from first principles quantum mechanics. For the spectral region of interest here, the best available potential energy surface is due to Partridge and Schwenke (PS) (*11*), who used known spectroscopic data to improve their high-accuracy *ab initio* surface.

It is possible to fit a dipole surface to experimental data (*12*); however, systematic tests of this procedure (*13*) strongly suggest that dipole surfaces constructed in this fashion are less reliable than those computed *ab initio*. This behavior is at least in part associated with the relatively large errors in experimentally determined intensities. The systematic errors discovered in the HITRAN intensities and described in I make the use of this data to construct dipole surfaces even more dubious. Therefore this work used PS's linelist (*14*), which employed their *ab initio* dipole surfaces. Concerns over the analytical representation of this surface (*15*), which we were only aware of after completing this work, will be discussed below.

A theoretically calculated linelists such as PS's yields following information:

1. The line position, $\tilde{\nu}_{nm}$ in cm^{-1}.
2. Line intensity, $\bar{S}_m^n$, in cm $\mathrm{molecule}^{-1}$.
3. Energy of lower state involved in the transition in cm^{-1}.
4. Total rotational quantum number of upper and lower states, J' and J''.
5. Rotational parity of upper and lower state, p' and p''.
6. Nuclear spin statistical weight, g.

This set of parameters is sufficient to calculate the intensity of a given transition as a function of temperature. The quantum numbers J, p and g are the only rigorous quantum numbers associated with a particular energy level. In practice PS's linelist labels each energy level with an approximate set of vibrational quantum numbers (v_1, v_2, v_3) and rotational quantum numbers (J, K_a, K_c). However, these full assignments have to be treated with caution as they are sometimes incorrect.

The PS linelist was used to give line parameters for the weak transitions not measurable experimentally in I. In practice there are a very large number of possible transitions and only those transitions with an intensity greater than 1×10^{-28} cm $\mathrm{molecule}^{-1}$ at 296 K were retained in the final list. This intensity cut-off is three orders of magnitude weaker than the weakest line measured in I and therefore resulted in a large number of extra lines.

Before discussing the details of our strong line–weak line strategy it is interesting to analyze the accuracy of the strong line intensities predicted by PS. Figure 1 compares intensities obtained at 296 K for the $2\nu + \delta$, $3\nu + \delta$, and 4ν polyads; a similar comparison for the 3ν polyad has been given elsewhere (*7*). For the $2\nu + \delta$ polyad, for which the PS linelist is the most reliable, PS's predictions strongly suggest that HITRAN systematically underestimates the water transition intensities. In this the PS results are in close agreement with the measurements of I. For the higher polyads the predictions of PS agree less well with the measurements of I but still, on average support the view that HITRAN underestimates the water transition intensities. However, for these higher polyads, the PS linelist displays clear systematic errors which correlate with the vibrational state being excited. This effect has recently been analysed by PS (*15*) who found that it was caused by the analytic fit of the *ab initio* dipole points. It should be noted that in this work the data for these (strong) transitions is taken from our measurements and not PS.

Assignment of both rigorous and approximate quantum numbers to the experimental lines measured in I is not straightforward (*16*) but is a necessary step in compiling the database so that, for example, temperatures other than those used in I can be modeled. Assignments were made using a combination of the PS empirically corrected linelist and the *ab initio* ZVPT linelist (*17*) using procedures developed for analyzing long-pathlength spectra (*16–18*).

In the absence of a reliable theory for predicting parameters which depend on pressure effects, these parameters were determined empirically using data from I. As shown in I, the measured air broadening parameters, γ_L(air), agree well with previous experimental values as tabulated in HITRAN. Figure 2 shows how these air broadening parameters behave as a function of the rotational and vibrational excitation. Although there is considerable scatter in the results, on average the parameters are found to be independent of the vibrational state excited and to depend approximately linearly on the rotational excitation of the lower state, J''.

Air broadening parameters for the experimental lines were set at the measured values reported in I. To obtain broadening parameters for the theoretical lines it was necessary to make a number of assumptions. It was assumed that γ_L(air) values are independent of the vibrational states involved in the transitions, are dependent on the lower rotational state via a formula derived from fits to the experimental data, and have a fixed temperature dependence. Furthermore, pressure shifts were assumed to be zero; in any case the measurements reported in I show these to be small, between 0.01 and 0.04 cm^{-1} atm^{-1}. These assumptions are necessary to be able to compile the linelist but it should be emphasized that they are only applied to weak lines, for which

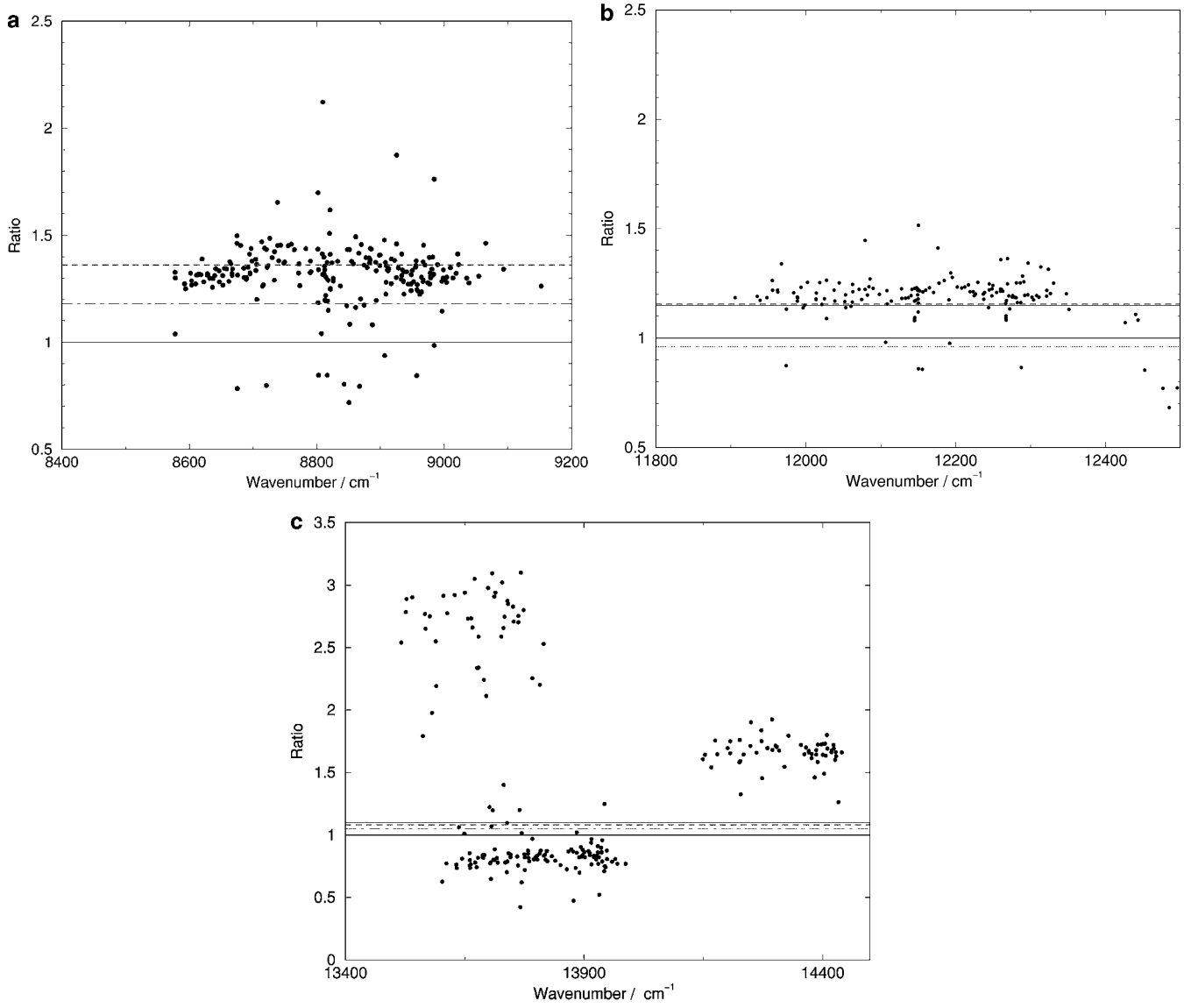

FIG. 1. The ratio of integrated line intensities, S_{mn}, from PS (*11*) to the corrected HITRAN data of Giver *et al.* (*8*) for $H_2{}^{16}O$ lines with intensities of more than 10^{-23} cm molecule^{-1}. The level of the unit ratio is indicated by the continous line, the dashed line gives the best fit to the present data, the dot–dash line gives the corresponding ratio for the uncorrected HITRAN-96 data, and the thin solid line gives the recommended scaling of Belmiloud *et al.* (*7*). (a) $2\nu + \delta$ polyad, (b) 3ν polyad, and (c) 4ν polyad.

pressure broadening effects are much less important. We used the following formula for the air broadening coefficient as a function of rotational state,

$$\gamma_L(\text{air}) = (296/T)^n(a - bJ(J+1)), \qquad (1)$$

where J is given by the minimum of J'' and 12, and the temperature dependence was fixed at the HITRAN value of $n = 0.68$. The parameters a and b were taken as 0.0916 cm^{-1} atm^{-1} and 0.00043 cm^{-1} atm^{-1}, respectively, by fitting to the J'' dependence of the lines in Fig. 2. The air broadening data in I were derived assuming the self- to air-broadening ratio $\gamma_L(H_2O)/\gamma_L(\text{air}) = 5.14$, and this ratio was used to generate $\gamma_L(H_2O)$ for both strong and weak lines.

3. CONSTRUCTION OF THE DATABASE

The ESA–WVR linelist was formed by merging theoretical lines with the lines measured in I. In most cases, lines for which measured data were available were removed from the theoretical linelist. In practice, for reasons given below, some of the weaker measured lines were removed instead. The final linelist is available in HITRAN 1996 format from http://www.badc.rl.ac.uk/data/esa-wv. For lines which already appear in the 1996 version of HITRAN, line positions were

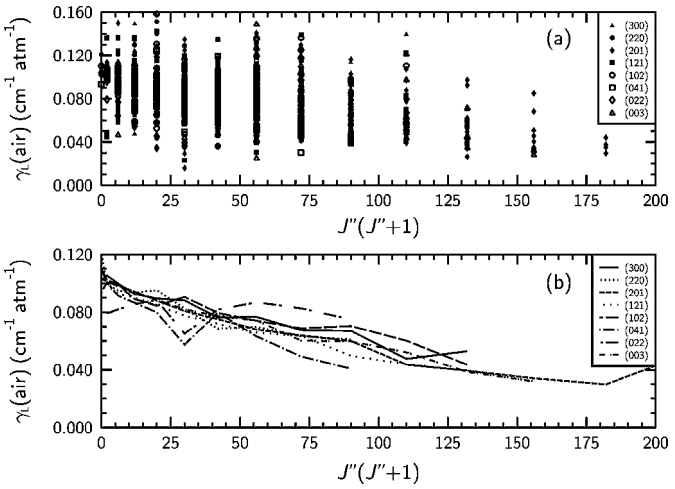

FIG. 2. Measured air-broadening paramaters, γ_L(air), as function of lower rotational state, J''. (a) All results, (b) Average values for a given J'' and upper vibrational state.

shifted to the HITRAN values as the HITRAN line positions were measured to higher accuracy than those reported in I and, more importantly, have the pressure shifts eliminated.

The spectrum of water has a pronounced band structure based on the underlying polyad structure of the energy levels. The present study covered four polyads and it was convenient to process the data for each polyad in turn. The summary in Table 1 shows that the 3ν polyad contains approximately the same number of transitions as the others combined. This polyad thus proved the most demanding.

When the experimental and theoretical linelists were combined a number of points had to be considered.

Not all the lines measured in I were assigned. Assignments are essential to determine the correct temperature dependence of the line parameters. We assigned most of the previously unassigned measured lines. In making these assignments we concentrated on getting the correct lower state energy and rotational quantum numbers as these parameters are crucial for determining absorption cross-sections as function of temperature. A full systematic assignment analysis of the new data based on long path-length spectra of pure water vapor recorded in the near infrared and visible, has been performed independently. This dataset has many more weak, unassigned lines and our new assignments will be reported as part of this work (*19*). Weak measured lines that could not be assigned were removed from the linelist and replaced by their theoretical counterparts.

Some of the lines measured in I proved to be unresolved blends of two or three lines. In many cases this problem was identified during the measurement procedure and appropriate numbers of line parameters characterized. However, it was

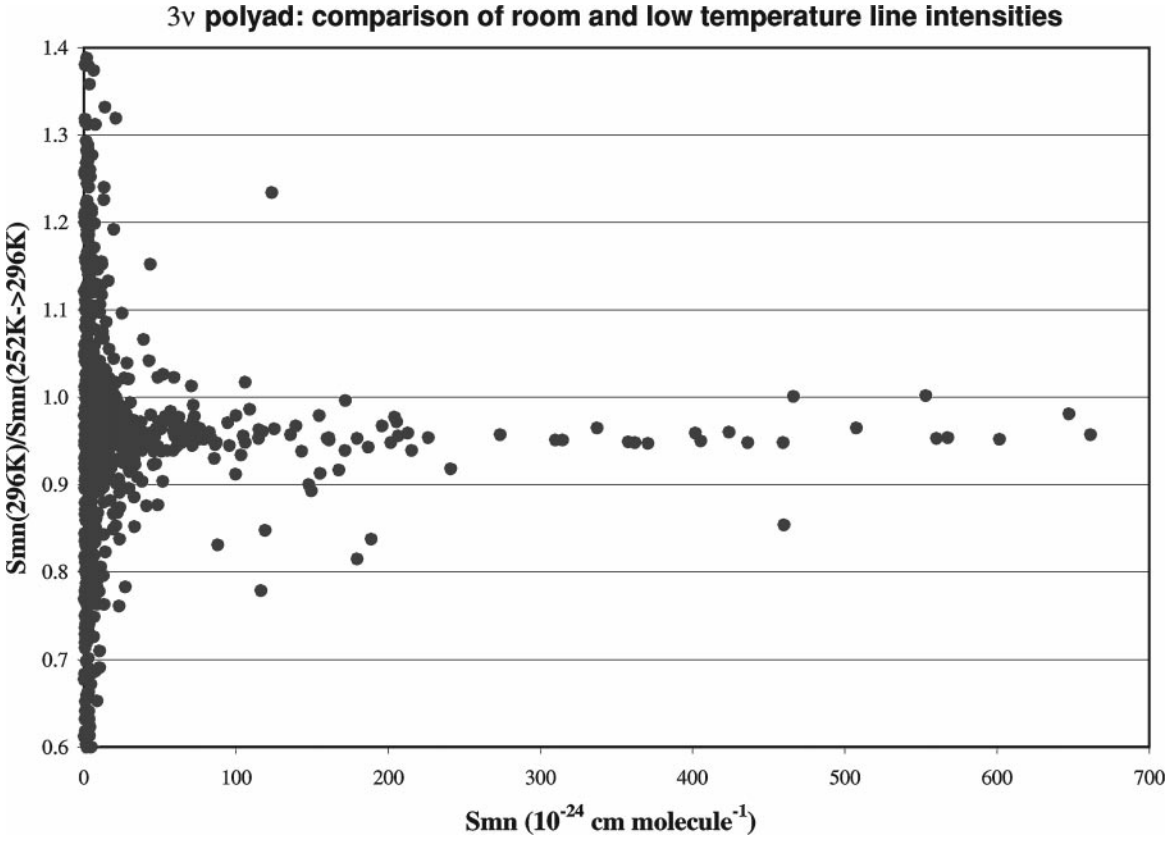

FIG. 3. Comparison of room-temperature ($T = 296$ K) and low-temperature ($T = 252$ K) intensity measurements for the 3ν polyad as a function of line intensity, S_{mn}.

TABLE 1
Summary of Lines Included in the Linelist by Polyad

Polyad	Range cm^{-1}	Number of strong lines measured	retained	Newly assigned	Total number of lines
$2\nu + \delta$	8592–9488	706	633	30	6040
	9488–9651	No strong lines			439
3ν	9651–11414	2447	1897	192	12430
	11414–11589	No strong lines			397
$3\nu + \delta$	11589–12752	889	715	134	6380
	12752–13403	No strong lines			1659
4ν	13403–14537	982	910	142	7958
	14537–15000	No strong lines			1297
Total	8592–15000	5034	4155	587	36600

apparent from comparison with the theoretical linelists that some blended transitions had been fitted with a single set of line parameters. Some blended lines have a dominant component or, in the case of pairs of quasi-degenerate ortho/para transitions, the same temperature dependence. The experimental data for these lines was retained in the linelist as a single line and labeled according to the stronger line. Both lines were removed from the theoretical linelist. In the few remaining cases we found rather broad weak lines which actually proved to have two or three components. These lines were removed from the experimental linelist as it was assumed that they were better modeled by theory.

A number of the transitions measured in I corresponded to the $H_2^{18}O$ isotopomer of water, which is present in natural abundance at 0.02%. Experimental transitions which could be assigned to $H_2^{18}O$ have been labeled using the HITRAN convention for denoting isotopomers. Some care was needed in doing this as it became apparent during the course of the study that a number of transitions assigned to $H_2^{18}O$ in HITRAN were actually weak $H_2^{16}O$ transitions. These transitions were reassigned with the appropriate $H_2^{16}O$ quantum numbers. In addition some lines in HITRAN have competing assignments to both $H_2^{16}O$ and $H_2^{18}O$. For these the $H_2^{16}O$ assignment was assumed; in nearly all cases this assumption could be shown to be correct on intensity grounds. The resulting number of remaining $H_2^{18}O$ measured lines is therefore fairly small: only 23 transitions, all in the 3ν polyad. Indeed, analysis of air-broadened natural water spectra is not a reliable way to extract data on $H_2^{18}O$. Isotopically enriched, long-pathlength FTS spectra of $H_2^{18}O$ are available (*20*) and are currently being analyzed for the 12 400- to 15 000-cm^{-1} range. No attempt was made to use a theoretical $H_2^{18}O$ linelist to supplement the experimental one.

For the stronger lines present in both the 296 K and 252 K spectra, the measured line intensities showed systematic differences of up to 5%. This shift was found to be independent of wavenumber, with the higher temperature measurements

TABLE 2
Integrated Band Intensities at 296 K for the Region 8600–15 000 cm^{-1}

Band	Experimental Number of Lines	Intensity cm molecule^{-1}	Total Number of Lines	Intensity cm molecule^{-1}	% theory
130	9	2.13(−22)	401	2.47(−22)	14.0
031	29	1.57(−22)	545	2.33(−22)	32.7
210	75	1.68(−21)	965	1.88(−21)	10.7
111	319	4.57(−20)	999	4.72(−20)	3.1
012	195	7.16(−22)	1051	8.67(−22)	17.5
060	3	1.43(−22)	743	1.51(−22)	5.6
140	4	2.53(−25)	854	9.08(−24)	97.2
041	144	4.60(−23)	1037	6.57(−23)	30.0
220	125	6.26(−23)	1129	8.85(−23)	29.2
121	324	2.62(−21)	1467	2.69(−21)	2.4
022	79	7.62(−23)	1352	1.02(−22)	25.4
300	268	1.67(−21)	2296	1.73(−21)	3.3
201	437	2.01(−20)	1748	2.02(−20)	0.5
102	240	6.08(−22)	295	6.09(−22)	0.1
003	278	2.31(−21)	1245	2.35(−21)	1.8
070	4	1.24(−24)	446	7.12(−24)	82.5
051	3	3.21(−24)	836	7.04(−24)	54.3
230	17	2.92(−24)	757	1.16(−23)	74.9
131	98	4.23(−23)	1085	4.97(−23)	15.0
032	3	6.91(−25)	777	6.28(−24)	89.0
310	95	6.42(−23)	1762	8.06(−23)	20.4
211	270	1.53(−21)	1273	1.54(−21)	0.8
112	116	5.11(−23)	126	5.11(−23)	0.0
013	124	1.02(−22)	879	1.06(−22)	4.0
240	4	5.41(−25)	619	3.70(−24)	85.4
141	9	1.47(−24)	574	3.68(−24)	60.1
042	5	2.51(−24)	535	4.81(−24)	47.8
320	27	8.07(−24)	1488	1.97(−23)	59.0
221	170	1.69(−22)	982	1.76(−22)	4.2
122	15	1.48(−24)	19	1.48(−24)	0.1
023	28	5.58(−24)	734	7.22(−24)	22.7
400	118	3.99(−23)	1170	4.96(−23)	19.6
301	248	1.19(−21)	1662	1.21(−21)	1.5
202	128	8.13(−23)	128	8.13(−23)	0.0
103	157	1.96(−22)	169	1.96(−22)	0.0
004	3	1.12(−24)	515	3.85(−24)	70.9
Other	0	0.0	3937	1.55(−23)	100.0
Total	4171	7.96(−20)	36600	8.20(−20)	2.9

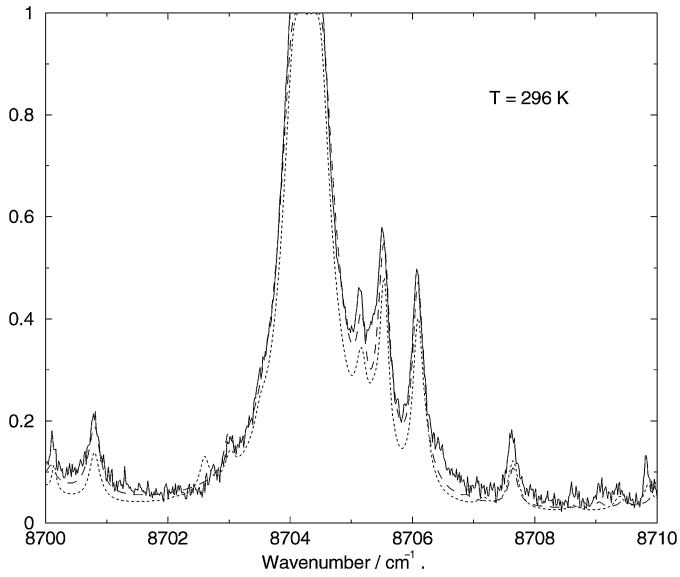

FIG. 4. Observed water–air spectrum in the $2\nu + \delta$ region with a 512-m pathlength and $T = 296$ K, solid line. Simulated spectra using ESA–WVR linelist, long–dashed line, and HITRAN, short-dashed line.

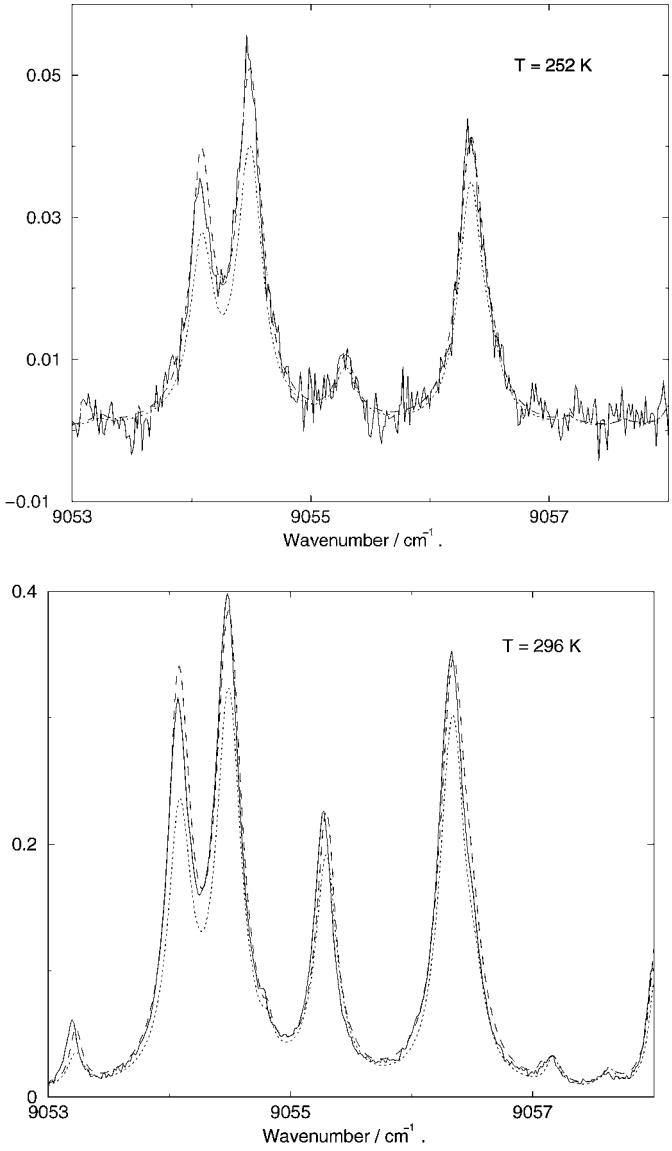

FIG. 5. Observed water–air spectrum in the $2\nu + \delta$ region with a 512-m pathlength, solid line. Simulated spectra using ESA–WVR linelist, long-dashed line, and HITRAN, short-dashed line. Upper: $T = 252$ K; lower: $T = 296$ K.

systematically giving slightly weaker transitions (see Fig. 3 for an example). This problem is almost certainly a result of difficulties associated with determining the water partial pressure in the water-air mixture, as discussed in I. In considering temperature effects, the high-accuracy partition function of Vidler and Tennyson (*21*) was used. In practice, for the temperatures considered here, this gave good agreement with other reported values (*1*, *11*).

In combining line values of parameters recorded at different temperatures, weighted averages were used. The combined intensity parameter was determined shifting the individual line intensities measured at 252 K, $S(252)$, to 296 K using the Boltzmann factors and then weighting the average using percentage errors. This had the effect of giving values intermediate between those from the two measurements. In practice, the averaged intensity parameters are closer to those measured at 296 K as these were determined with a smaller percentage error.

Table 1 summarizes the linelist by polyad and includes data for the interpolyad regions, for which there are still weak transitions. Using the ESA–WVR linelist it is possible to estimate integrated band intensity at 296 K for the vibrational states which contribute significantly to each of the polyads. Results of this analysis are given in Table 2, which gives results for both the measurements of I and the total contribution. The percentage given by theory to the latter is also tabulated. The results in Table 2 only cover lines which lie in the frequency range 8600–15 000 cm^{-1}, but

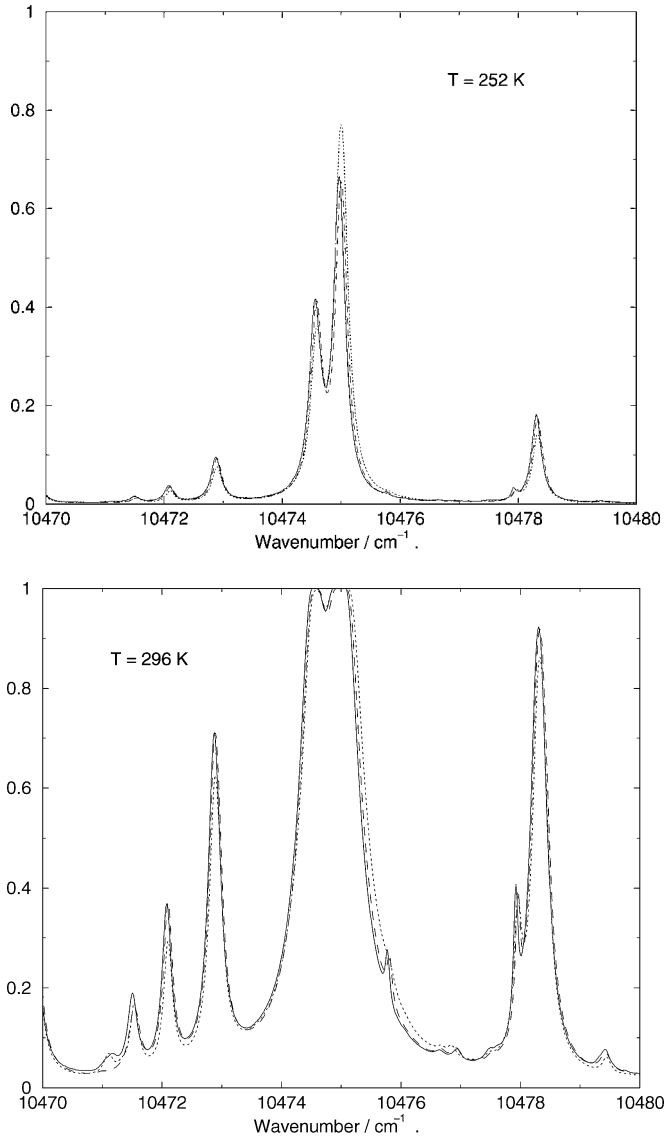

FIG. 6. Observed water–air spectrum in the 3ν region with a 512-m pathlength, solid line. Simulated spectra using ESA–WVR linelist, long-dashed line, and HITRAN, short-dashed line. Upper: $T = 252$ K; lower: $T = 296$ K.

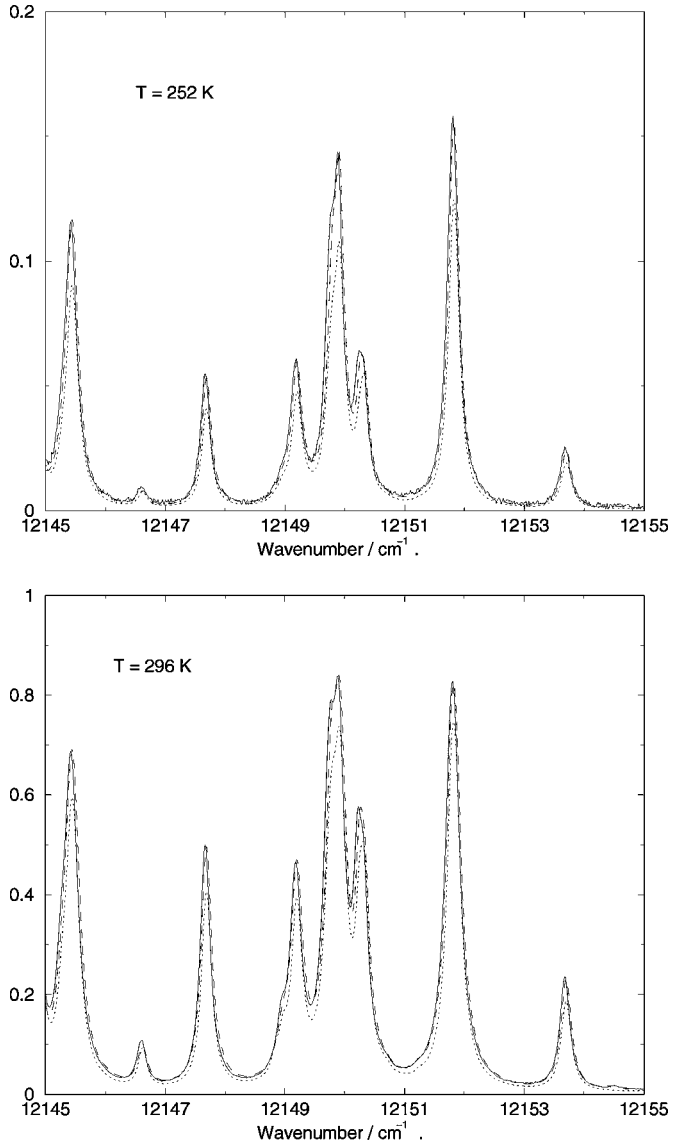

FIG. 7. Observed water–air spectrum in the $3\nu + \delta$ region with a 512-m pathlength, solid line. Simulated spectra using ESA–WVR linelist, long-dashed line, and HITRAN, short-dashed line. Upper: $T = 252$ K; lower: $T = 296$ K.

this should not be an important approximation for nearly all the bands considered.

4. VALIDATION

The linelists were validated by showing that they could be used to regenerate the experimental data as a function of temperature and path-length. For this purpose the RFM software package (*22*) was used to generate synthetic spectra.

Two methods were used to assess the data. Detailed observed and calculated spectra were plotted over the entire frequency range considered. Samples comparisons are given in Figs. 4–9. For comparison the figures also give spectra generated using HITRAN 96 data (*1*). For this we have used the uncorrected data; for reasons discussed elsewhere (*7*), use of the recent corrections due to Givers *et al.* (*8*) does not significantly alter the conclusions made below.

It can be seen from the figures that the agreement between observed and synthesized spectra is generally good and that the ESA–WVR linelist gives significantly better results than HITRAN. In some regions, see Fig. 8 for example, the effect of shifting our measured frequencies to HITRAN values can be clearly seen. The only region where systematic differences between our measurements and the synthetic spectra generated using ESA–WVR were identified was 8700–8750 cm^{-1}; see Fig. 5. Here it appears that there were problems in correctly determining the spectral baseline during the experimental measurements. This is probably due to the large number of strong or saturated lines in this region and the detector cut-off.

The second, more quantitative, method of assessing the data was to compare the integrated absorption intensities of the measured and synthetic spectra region by region as a function of path-length and temperature. For this purpose integration was performed over the approximate center of each polyad although regions in which other species might corrupt the measured spectra, in particular 14 000–14 500 cm^{-1}, were excluded. Results are given in Table 3, from which it can be seen that measured and synthetic spectra are in close agreement. The only region where the disagreement is greater than 5% is the 4ν polyad at 252 K. This is the weakest spectrum analyzed and, as can be seen from Fig. 9, the signal-to-noise of the measurements in this region is lower, even at $T = 296$ K. At 252 K much of the spectrum is dominated by noise; integrating over this noise is the main cause of this error.

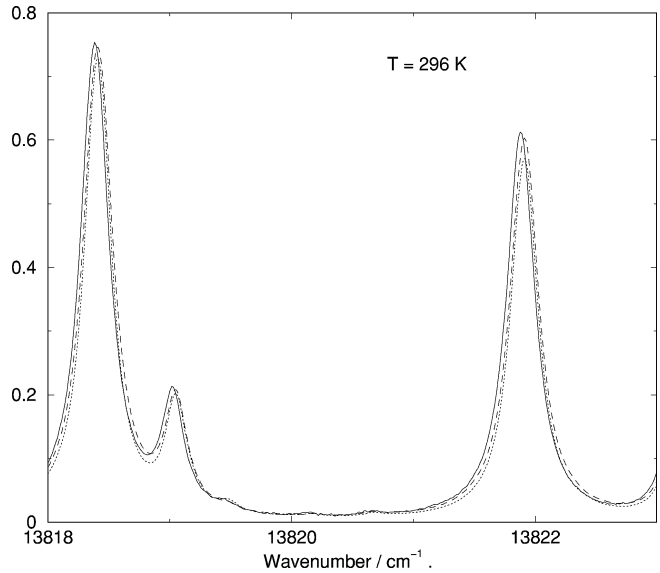

FIG. 8. Observed water–air spectrum in the 4ν region with a 512-m pathlength and $T = 296$ K, solid line. Simulated spectra using ESA–WVR linelist, long-dashed line, and HITRAN, short-dashed line.

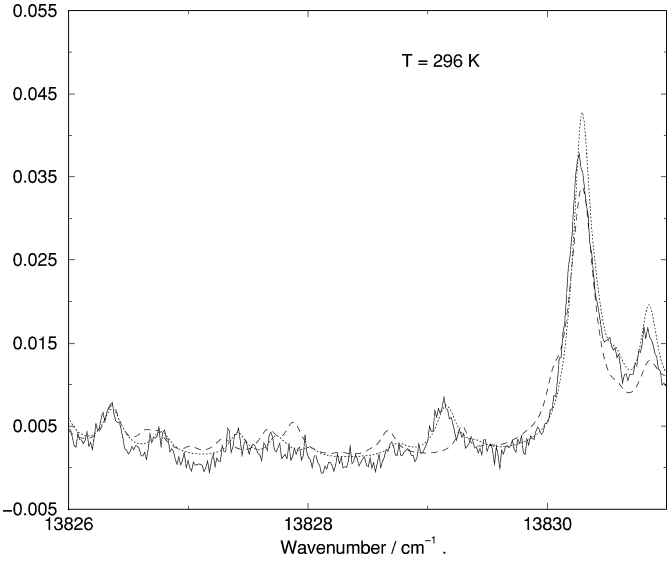

FIG. 9. Observed water–air spectrum in a weak part of the 4ν region with a 512-m pathlength and $T = 296$ K, solid line. Simulated spectra using ESA–WVR linelist, long-dashed line, and HITRAN, short-dashed line.

A basic assumption of our method, which is only partially tested by our validation procedure, is that the theoretical representation of the intensities of the weak lines is as accurate as the theoretical representation of the strong lines. The recent results of Schwenke and Partridge (*15*) concerning the water dipole surface call this assumption into question. Even though the theoretical lines account for less than 3% of the integrated intensity at 296 K (see Table 2), this is still an important issue and one we plan continued work on.

In conclusion, we have combined the long-pathlength experimental measurements reported in I with a high-quality calculated linelist to provide a comprehensive under database covering near-infrared and visible wavelengths. This database, which we call ESA–WVR, is freely available. As discussed previously (*7*, *10*), use of this database in place of the data in HITRAN 96 (*1*) or the recently corrected version of this database (*8*), gives a significant increase in the amount of absorption due to water vapor at these wavelengths. This increase arises from two causes: the increased intensities of the strong lines, found in the new experiments reported in I, and the extra absorption due to the inclusion of the many additional weak lines. Model atmospheric calculations now under way (*23*) lend strong support to this conclusion.

TABLE 3
Integrated Absorption Intensity by Polyad in Arbitrary Units: Comparison of Observed and Linelist-Generated Spectra

Polyad	Range/cm^{-1}	Temperature = 296K			Temperature = 252K		
		Obs.	Calc.	Diff.	Obs.	Calc.	Diff.
$2\nu + \delta$	8800–9400	89.610	87.015	2.9%	22.450	22.022	1.1%
3ν	10000–11200	141.556	142.261	0.5%	24.995	24.126	3.5%
$3\nu + \delta$	11900–12400	15.702	15.706	0.0%	1.738	1.719	1.1%
4ν	13600–14000	13.650	13.942	2.1%	1.328	1.492	11%

ACKNOWLEDGMENTS

We thank the U.K. Natural Environment Research Council (Grants GR3/11097, GR3/11674) and the European Space Agency (Contract 13312/99/NL/SF) for support. We thank J. Brault and O. L. Polyansky for help and advice, Martin Wickett of SERCO UK Ltd for undertaking the project management, and D. W. Schwenke for supplying results in advance of publication.

REFERENCES

1. L. S. Rothman, C. P. Rinsland, A. Goldman, S. T. Massie, D. P. Edwards, J.-M. Flaud, A. Perrin, C. Camy-Peyret, V. Dana, J.-Y. Mandin, J. Schroeder, A. McCann, R. R. Gamache, R. B. Wattson, K. Yoshino, K. V. Chance, K. W. Jucks, L. R. Brown, V. Nemtchinov, and P. Varanasi, *J. Quant. Spectrosc. Radiat. Transfer* **60,** 665–710 (1998).
2. N. Jacquinet-Husson *et al.*, *J. Quant. Spectrosc. Radiat. Transfer* **62,** 205–254 (1999).
3. C. Camy-Peyret, J.-M. Flaud, J.-Y. Mandin, J.-P. Chevillard, J. Brault, D. R. Ramsay, and M. Vervloet, *J. Mol. Spectrosc.* **113,** 208–228 (1985).
4. J.-Y. Mandin, J.-P. Chevillard, C. Camy-Peyret, and J.-M. Flaud, *J. Mol. Spectrosc.* **116,** 167–190 (1986).
5. J.-Y. Mandin, J.-P. Chevillard, J.-M. Flaud, and C. Camy-Peyret, *Can. J. Phys.* **66,** 997–1011 (1988).
6. J.-P. Chevillard, J.-Y. Mandin, J.-M. Flaud, and C. Camy-Peyret, *Can. J. Phys.* **67,** 1065–1084 (1989).
7. D. Belmiloud, R. Schermaul, K. Smith, N. F. Zobov, J. Brault, R. C. M. Learner, D. A. Newnham, and J. Tennyson, *Geophys. Res. Lett.* **27,** 3703–3706 (2000).
8. L. P. Giver, C. Chackerian Jr., and P. Varanasi, *J. Quant. Spectrosc. Radiat. Transfer* **66,** 101–105 (2000).
9. R. Schermaul, R. C. M. Learner, D. A. Newnham, R. G. Williams, J. Ballard, N. F. Zobov, D. Belmiloud, and J. Tennyson, *J. Mol. Spectrosc.* **208,** 32–42 (2001).
10. R. C. M. Learner, W. Zhong, J. D. Haigh, D. Belmiloud, and J. Clarke, *Geophys. Res. Lett.* **26,** 3609–3612 (1999).
11. H. Partridge and D. W. Schwenke, *J. Chem. Phys.* **106,** 4618–4639 (1997).
12. R. B. Wattson and L. S. Rothman, *J. Quant. Spectrosc. Radiat. Transfer* **48,** 763-?? (1992).
13. A. E. Lynas-Gray, S. Miller, and J. Tennyson, *J. Mol. Spectrosc.* **169,** 458–467 (1995).
14. D. W. Schwenke, available at http://george.arc.nasa.gov/∼dschwenke/h2o/h2o.html.
15. D. W. Schwenke and H. Partridge, *J. Chem. Phys.* **113,** 6592–6597 (2000).
16. O. L. Polyansky, N. F. Zobov, S. Viti, and J. Tennyson, *J. Mol. Spectrosc.* **189,** 291–300 (1998).
17. O. L. Polyansky, J. Tennyson, and N. F. Zobov, *Spectrochimica Acta*. **55A,** 659–693 (1999).
18. M. Carleer, A. Jenouvrier, A.-C. Vandaele, P. F. Bernath, M. F. Mérienne, R. Colin, N. F. Zobov, O. L. Polyansky, J. Tennyson, and A. V. Savin, *J. Chem. Phys.* **111,** 2444–2450 (1999).
19. R. Schermaul, R. C. M. Learner, J. W. Brault, A. A. D. Canas, O. L. Polyansky, N. F. Zobov, D. Belmiloud, and J. Tennyson, submitted for publication.
20. J.-P. Chevillar, J.-Y. Mandin, J.-M. Flaud, and C. Camy-Peyret, *Can. J. Phys.* **65,** 777–789 (1987).
21. M. Vidler and J. Tennyson, *J. Chem. Phys.* **113,** 9766–9771 (2000).
22. A. Dudhia, RFM package, http://www.atm.ox.ac.uk/RFM.
23. W. Zhong, J. D. Haigh, D. Belmiloud, R. Schermaul, and J. Tennyson, *Quart. J. Roy. Metr. Soc.*, in press.